

1 **Simulated responses of the West African monsoon and**
2 **zonal-mean tropical precipitation to early Holocene orbital**
3 **forcing**

4 **Jane E. Smyth¹, Spencer A. Hill^{2,3}, Yi Ming⁴**

5 ¹Program in Atmospheric and Oceanic Sciences, Princeton University, Princeton, New Jersey

6 ²Department of Atmospheric and Oceanic Sciences, University of California, Los Angeles

7 ³Division of Geological and Planetary Sciences, California Institute of Technology, Pasadena, California

8 ⁴Geophysical Fluid Dynamics Laboratory/NOAA, Princeton, New Jersey

9 **Key Points:**

- 10 • The West African monsoon, which expands northward in response to early Holocene
11 orbital forcing, does not behave as a simple extension of the zonal-mean ITCZ.
12 • The ITCZ either responds weakly or shifts southward in boreal summer, counter to the
13 prevailing energetic framework.
14 • Anomalous southward energy fluxes manifest as increased total gross moist stability
15 rather than a northward ITCZ shift.

Corresponding author: Jane E. Smyth, jsmyth@princeton.edu

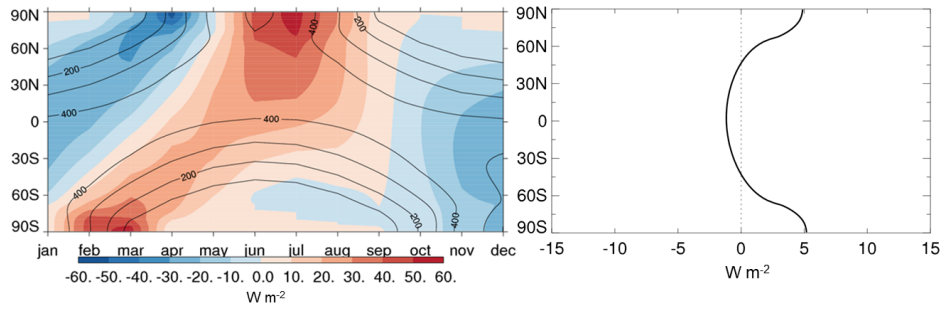
Abstract

This study seeks to improve our mechanistic understanding of how the insolation changes associated with orbital forcing impact the West African monsoon and zonal mean tropical precipitation. We impose early Holocene orbital parameters in simulations with the Geophysical Fluid Dynamics Laboratory AM2.1 atmospheric general circulation model, either with sea surface temperatures prescribed at present-day values or with a 50-meter thermodynamic slab ocean. In both cases, West African Monsoon rainfall expands northward, but in neither case does the summer zonal mean Intertropical Convergence Zone (ITCZ) do the same – responding weakly with prescribed SSTs and shifting southward with a slab ocean lower boundary. This contradicts expectations from the conventional energetic framework for the ITCZ location, given anomalous southward energy fluxes in the deep tropics. These anomalous energy fluxes are not accomplished by a stronger Hadley circulation; instead, they arise from an increase in total gross moist stability in the northern tropics.

1 Introduction

Ample paleoclimate data indicates that 10,000 years ago (10 ka), near the beginning of the Holocene Epoch, much of Northern Africa was substantially wetter than today [e.g., *Tierney et al.*, 2017, and references therein]. This was the peak of the African Humid Period (15 to 5 ka), when increased humidity and vegetation characterized the modern Sahara [*deMenocal*, 2015]. Past modeling studies imply that this largely resulted from an intensification and northward expansion of the West African monsoon [*Joussame et al.*, 1999]. At present, appreciable monsoon rainfall extends only as far north as the Sahel, the transitional region separating the Sahara Desert from the savannas to the south.

Precession is the primary orbital signal modulating Holocene insolation and rainfall over Africa relative to modern conditions [*DeMenocal and Tierney*, 2012]. At 10 ka, perihelion occurred during Northern Hemisphere (NH) summer, as opposed to NH winter today. This intensified the NH seasonal cycle of insolation and weakened the SH seasonal cycle (Fig. 1). A more oblique orbit at 10 ka relative to present modified insolation to a lesser extent, and was responsible for any annual mean insolation changes (Fig. 1, right panel) [*Luan et al.*, 2012]. Meridional gradients in insolation or surface properties can influence monsoons, which are initiated by meridional gradients of subcloud moist static energy (MSE) (nearly equivalently, of subcloud equivalent potential temperature) [*Emanuel*, 1995; *Hurley and Boos*, 2013].



47 **Figure 1.** (Left) Annual cycle of insolation (black contours) at present and (color shading) anomalies
 48 applied in the 10 ka simulations. (Right) annual mean 10 ka insolation anomalies. All in W m^{-2}

49 Based on previous studies linking anomalous cross equatorial energy fluxes to the po-
 50 sition of the zonal mean Intertropical Convergence Zone (ITCZ), one would expect this or-
 51 bitally driven insolation change to shift the ITCZ northward and strengthen its precipitation
 52 during NH summer [Schneider *et al.*, 2014; Bischoff *et al.*, 2017]. However, though ITCZ re-
 53 sponses to 10 ka-like precessional forcing are generally northward in fully coupled general cir-
 54 culation models (GCMs), they are often southward in slab-ocean simulations, and in more ide-
 55 alized models the direction is sensitive to the land-ocean configuration [Merlis *et al.*, 2013a,c;
 56 Liu *et al.*, 2017]. Liu *et al.* [2017] described that in nine of twelve coupled models forced with
 57 mid-Holocene orbital parameters, northward ocean heat transport drove a compensating south-
 58 ward atmospheric heat transport, which manifested as a northward ITCZ shift. Three coupled
 59 models and a slab ocean model displayed counterintuitive southward ITCZ shifts, for which
 60 a physical mechanism was not determined. Further analysis is needed to assess the plausibil-
 61 ity of this response and to explicate the underlying processes.

62 It is also not clear how much an individual continental monsoon system such as the West
 63 African Monsoon is influenced by the aforementioned zonal-mean constraints [Roberts *et al.*,
 64 2017] or even by the behavior of the adjacent oceanic ITCZ. Therefore, a particular focus is
 65 how the impacts of the imposed insolation gradient on dynamics and rainfall differ between
 66 the Sahel and the adjacent Atlantic Ocean.

67 **2 Experimental Design**

68 To clarify the influence of early Holocene orbital forcing on the West African monsoon
 69 and the zonal mean climate, we present results from four simulations performed using the Geo-

70 physical Fluid Dynamics Laboratory AM2.1 atmospheric general circulation model [*GFDL*
71 *Global Atmospheric Model Development Team, 2004*]: with either modern or 10 ka orbital pa-
72 rameters, and with either prescribed SSTs or a 50-meter slab ocean. The prescribed SSTs are
73 the climatological annual cycle from the Reynolds Optimum Interpolation dataset [*Reynolds*
74 *et al., 2002*] averaged over 1980-1999. The control AM2.1 simulation with a fixed annual cy-
75 cle of SSTs captures the main features of the observed modern climatology over the Sahel [*Hill*
76 *et al., 2017*]. In the 50-meter slab ocean configuration, SSTs are allowed to vary with the at-
77 mospheric forcing, and a prescribed horizontal ocean heat flux is calibrated to reproduce present-
78 day SSTs in the control simulation. The choice of idealized ocean components is intended to
79 clarify the role of the SST field in the zonal mean and regional climate response, without the
80 complicating influence of ocean dynamics. The model's land configuration does not feature
81 dynamic vegetation, so associated albedo and soil moisture feedbacks which intensify the mon-
82 soon response are muted [e.g., *Patricola and Cook, 2007*]. As such, both experiments under-
83 estimate the regional rainfall response compared to paleoclimate proxies [*Tierney et al., 2011*].
84 We performed two additional simulations with only 10 ka obliquity or precession; the latter
85 is dominant in the hydrological response (not shown).

86 The prescribed SST simulations span 17 years, with averages taken over the last 16 years.
87 The slab ocean simulations span 40 years, with averages taken over the last 20 years. We fo-
88 cus primarily on boreal summer (June, July, August, or JJA) mean results, since this spans the
89 period when the imposed insolation forcing is greatest in the tropics as well as the onset of
90 the modern West African monsoon season. We also briefly discuss the annual mean response.
91 Region-mean quantities were computed for the Sahel (land area within the domain 10 to 20°
92 N, 18° W to 40° E) and for the Atlantic ITCZ (ocean area within the domain 0 to 20° N, 60
93 to 15° W). All vertically defined quantities use pressure-interpolated data, and these results
94 do not differ importantly from those using data on model-native coordinates (not shown).

95 **3 Results**

96 **3.1 Atlantic ITCZ and Sahel Responses**

97 In both simulations with 10 ka orbital parameters, the precipitation over the Sahel in-
98 creases, in some places on the order of 100% (Fig. 2a). This can be interpreted as a north-
99 ward expansion of the monsoon and is in qualitative agreement with paleoclimate proxies. Pre-
100 cipitation increases over West Africa by up to 2-3 mm day⁻¹ in the prescribed SSTs case and

up to $3\text{--}6\text{ mm day}^{-1}$ in the slab ocean case. Associated near-surface MSE maxima also shift northward (not shown), consistent with the argument that the two features be nearly coincident [Prive and Plumb, 2007]. In contrast, precipitation decreases over the Atlantic ITCZ sector with both ocean configurations (Fig. 2a).

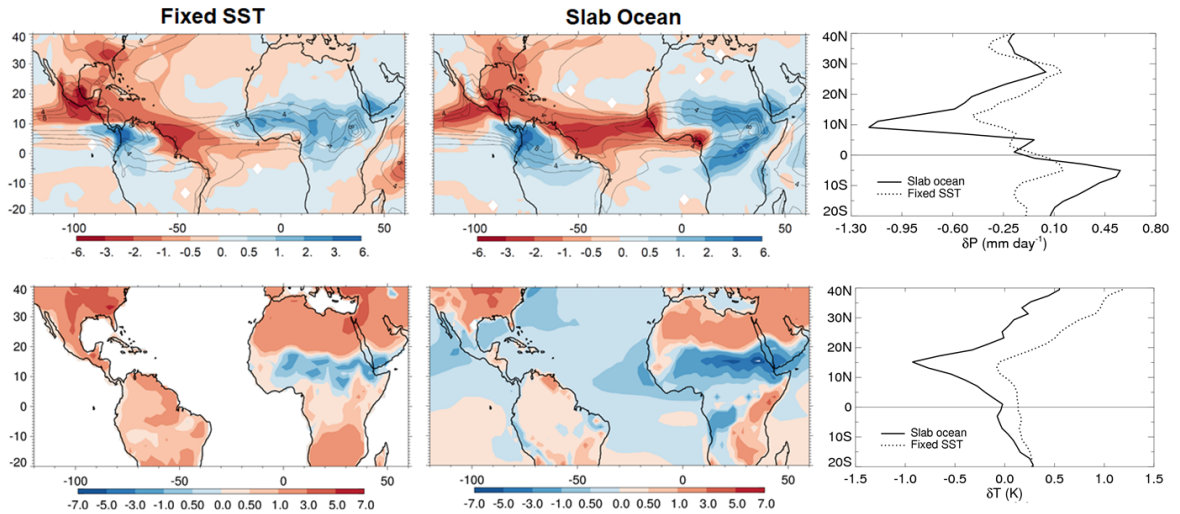


Figure 2. (Top row) JJA precipitation anomalies (10 ka-control , mm day^{-1}) in the fixed SSTs and slab ocean experiments. In the right panel, precipitation anomalies are averaged over all longitudes. (Bottom row) As above, but for temperature anomalies (K). The green boxes delimit the North Atlantic ITCZ region and the Sahel region, which are assessed in Fig. 3 with ocean-only and land-only regional averages, respectively. The color bar intervals are pseudo-logarithmic.

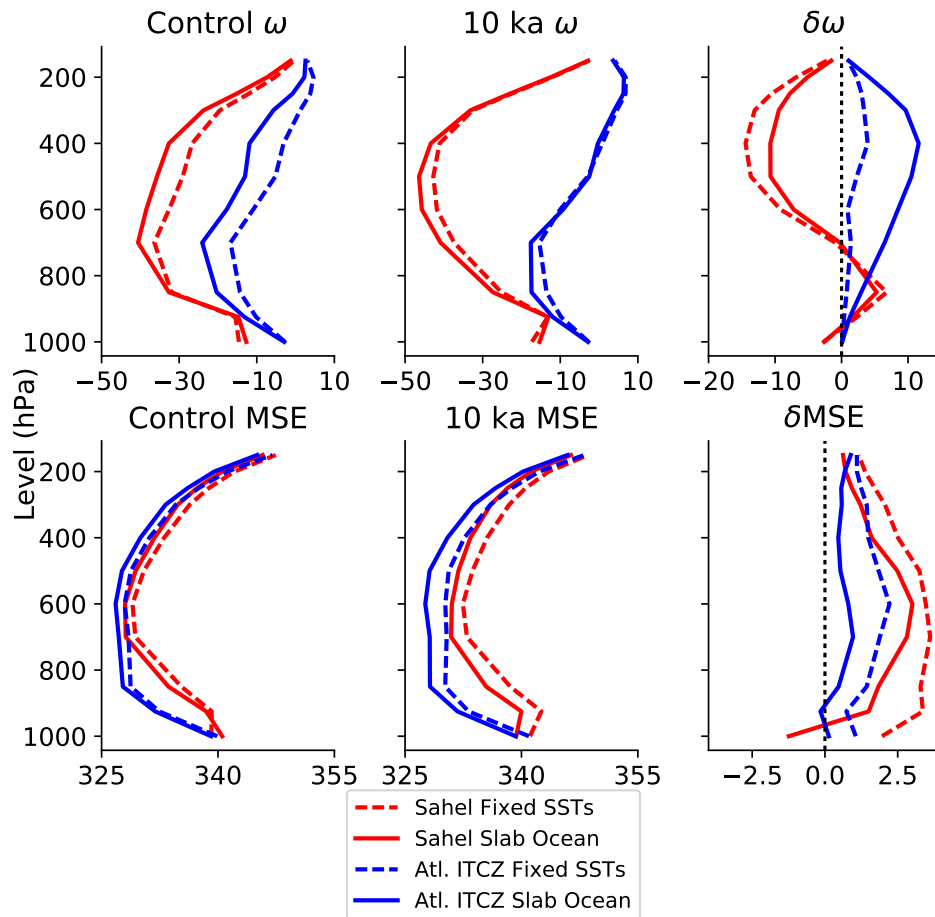
JJA surface temperatures decrease over the Sahel in the 10 ka simulations as precipitation increases, despite the insolation forcing (Fig. 2b). In a supply-limited evaporative regime such as the semi-arid Sahel, surface temperature and precipitation are generally tightly anti-correlated due to the impact of rainfall on the surface energy budget [e.g., Berg *et al.*, 2015]. In the prescribed SSTs case, the maximum cooling over the Sahel is between 1 and 2 K, and in the slab ocean experiment, the Sahel cools by up to 7 K (Fig. 2b). In the slab ocean simulation, cold Atlantic SST anomalies off the West coast of Africa during JJA reduce the cross-equatorial SST gradient. The positive insolation anomaly peaks in June, but due to the relatively deep, 50-meter mixed layer in the slab ocean simulations, the Atlantic SST response lags the insolation by 2–3 months (not shown), such that JJA SSTs actually cool relative to the present day [Donohoe *et al.*, 2014]. The precipitation response is similarly phase-lagged, due to the strong control over tropical oceans of SSTs on rainfall [e.g., Neelin and Held, 1987]. How-

122 ever, over the Sahel, the maximum precipitation anomaly occurs in JJA, in phase with the in-
 123 solation anomaly, presumably due to the low land heat capacity.

124 We now analyze terms of the column-integrated MSE budget in the Sahel and Atlantic
 125 regions; see e.g., *Hill et al.* [2017] Section 4(a) for a summary of the underlying theory. Fig.
 126 3 shows the regionally and seasonally averaged vertical velocity in pressure coordinates, ω ,
 127 as well as the vertical MSE profile. Over the Sahel, anomalous ascent above approximately
 128 700 hPa corresponds to a deepening of the circulation and greater vertical export of MSE. The
 129 JJA subcloud (850 hPa) meridional MSE gradient decreases over the Sahel in the 10 ka sim-
 130 ulations (not shown), which reduces horizontal MSE advection and necessitates more verti-
 131 cal MSE export. Consequently, the ascent profile deepens over the Sahel (Fig. 3b). There is
 132 a zero crossing in the ω anomaly profile over the Sahel only, and it occurs near the minimum
 133 (~ 700 hPa) in the MSE profile (Fig. 3), likely because this is where the static stability ($\partial MSE/\partial p$)
 134 changes sign [*Hill et al.*, 2017]. The combined precipitation, circulation, and energetic responses
 135 over the Sahel with either lower boundary condition bear resemblance to those induced by uni-
 136 form SST cooling in AM2.1 described by *Hill et al.* [2017, c.f. their Fig. 13].

140 Over the Atlantic sector, the vertical velocity weakens at all altitudes, with the strongest
 141 weakening at 400 hPa with both ocean configurations. This upper tropospheric descent im-
 142 plies a shallowing of the circulation, and thus a reduction in the vertical export of MSE. The
 143 lack of a dipole structure in $\delta\omega$ over the Atlantic suggests distinct dynamical mechanisms in
 144 the two regions. The dipole response over the Sahel may be locally forced by a change in the
 145 horizontal MSE gradient, while the $\delta\omega$ profile over the Atlantic may be a manifestation of the
 146 large-scale circulation adjustment. The North Atlantic vertical velocity weakens much more
 147 in the slab ocean experiment than the fixed SSTs experiment, and is consistent with the Hadley
 148 cell adjustment described in Section 3.2.2.

149 The anomalous descent over the Atlantic ITCZ sector motivated a surface energy bud-
 150 get analysis. Averaged over this region, an anomalous energy flux into the ocean (driven by
 151 shortwave and latent heat) outweighs the positive solar forcing at TOA (not shown). To first
 152 order, the reduced upward latent heat flux (-9.51 and -6.81 W m^{-2} in the fixed SST and slab
 153 ocean experiments, respectively) is caused by a weakening of the prevailing easterlies. The
 154 net-column cooling is amplified in the slab ocean experiment (shortwave flux anomaly of -16.1
 155 W m^{-2} , versus -10.1 W m^{-2} in the fixed SSTs experiment) due to the phase lag of the SSTs



137 **Figure 3.** JJA vertical profiles of (top row) ω (hPa/day) and (bottom row) MSE (K) in the control and 10 ka
 138 simulations, and their anomalies (10 ka - control). Results are averaged over the Sahel (10° to 20° N; 18° W
 139 to 40° E) and North Atlantic ITCZ (0° to 20° N; 60° to 15° W) regions.

156 relative to the insolation forcing (not shown). The decrease of net energetic forcing over the
 157 North Atlantic sector is consistent with weakened convection there [c.f., *Neelin and Held, 1987*].

158 The vertical structure of ω varies more between regions than the MSE profile (Fig. 3)
 159 [c.f., *Back and Bretherton, 2006*]. The distinct ω responses over the North Atlantic (0 to 20°
 160 N, 60° W to 15° W) and the Sahel (10 to 20° N, 18° W to 40° E) in JJA imply an anomalous
 161 zonal circulation, and a consequent suppression of precipitation over the North Atlantic
 162 sector. The subcloud MSE increases more over the Sahel than over the tropical North Atlantic
 163 with both ocean configurations (Fig. 3), and is associated with an enhanced monsoon circu-
 164 lation that shifts precipitation from ocean to land (Fig. 2).

165 **3.2 Zonal Mean Response**

166 Despite enhanced JJA NH insolation and associated southward anomalous cross-equatorial
 167 energy fluxes (discussed below), the zonal-mean ITCZ shifts southward in JJA in both 10 ka
 168 simulations, though to a much lesser extent in the fixed SSTs case (Fig. 2, right column). This
 169 runs counter to the prediction of energy flux equator theory, the results of many fully coupled
 170 GCMs [*Liu et al.*, 2017], and the locally northward rainfall migration over North Africa pre-
 171 viously described. The zonal mean precipitation is more suppressed in the NH than it is en-
 172 hanced in the SH (i.e., it is not a symmetric ITCZ shift), particularly in the slab ocean case.

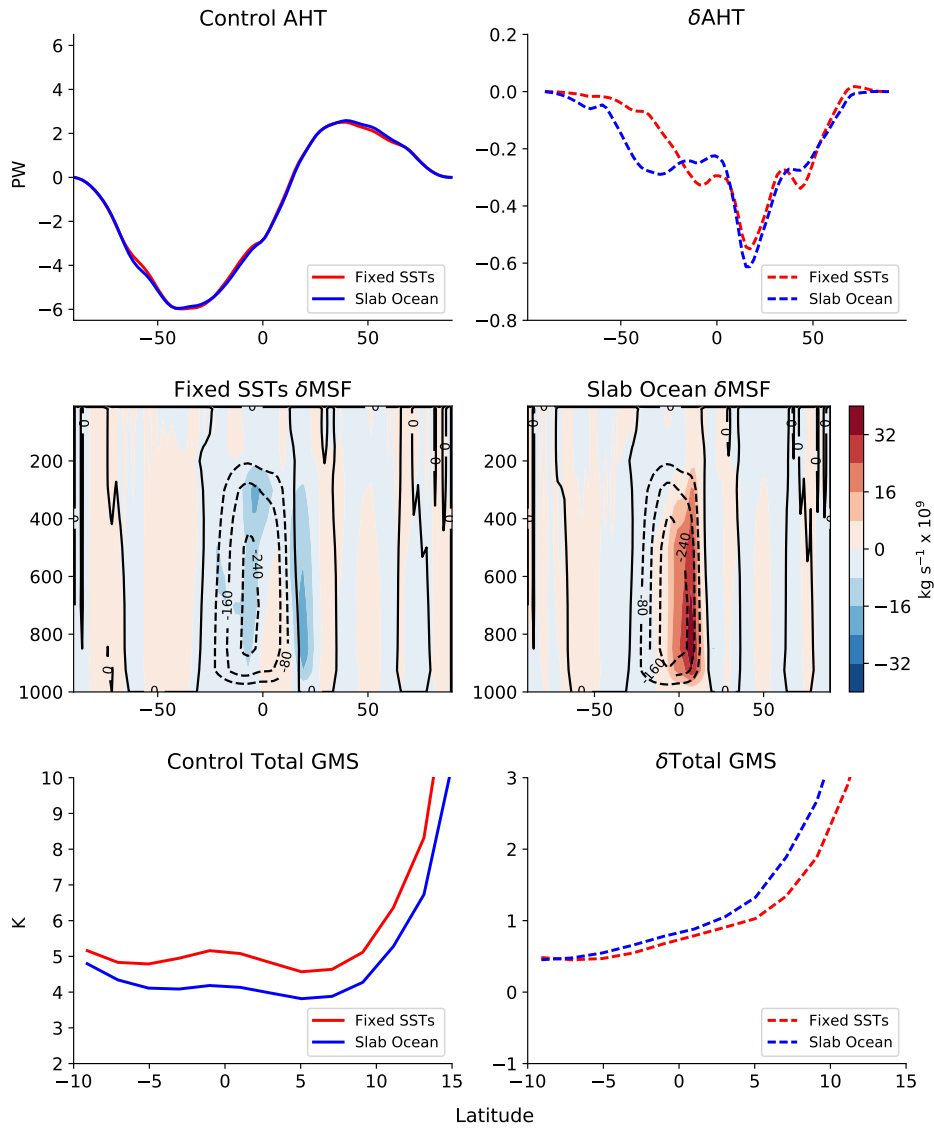
173 **3.2.1 Atmospheric Heat Transport**

174 The total atmospheric heat transport (AHT) is the zonally and meridionally integrated
 175 net energetic forcing term (equal to the total atmospheric energy flux divergence), which com-
 176 prises the sum of the top-of-atmosphere radiative and surface radiative, sensible heat, and la-
 177 tent heat fluxes into the atmosphere [e.g., Eq. A4 of *Hill et al.*, 2015]. As alluded to above,
 178 the 10 ka forcing induces anomalous southward energy transport throughout the tropics, peak-
 179 ing at ~ 0.6 PW near 15°N in both fixed SSTs and slab ocean cases (Fig. 4). The total gross
 180 moist stability is the ratio of $\text{AHT}(\phi)$ to the mass transport $\Psi(\phi)$ integrated to the pressure height
 181 of maximum intensity [*Kang et al.*, 2009].

187 **3.2.2 Hadley Circulation**

188 Based on the zonal mean meridional streamfunction [calculated c.f. Eq. A5 of *Hill et al.*,
 189 2015], the JJA southward energy flux is not accomplished by a stronger Hadley cell mass flux
 190 in either experiment (Fig. 4). The JJA mass flux does not change appreciably in the prescribed
 191 SSTs experiment, and the circulation actually weakens in the slab ocean case with a maximum
 192 magnitude of $35 - 40 \times 10^9 \text{ kg s}^{-1}$ (approximately 20%).

193 The Hadley circulation is governed by different physical regimes throughout the seasonal
 194 cycle, following variations in the value of the local Rossby number (Ro), defined as the neg-
 195 ative ratio of the relative and planetary vorticities [*Merlis et al.*, 2013a]. In the slab ocean ex-
 196 periment, the JJA Hadley cell weakens only in the NH ascending branch, through a secondary
 197 clockwise circulation that opposes the climatological overturning (Fig. 4). This is consistent
 198 with a regime in which the summer-hemisphere flank of the cross-equatorial Hadley cell con-
 199 serves angular momentum ($\text{Ro} \approx 1$) [*Merlis et al.*, 2013a]. In this regime, the Hadley cell re-



182 **Figure 4.** Results from the JJA zonal mean energetic analysis. (Top row) Atmospheric heat transport
 183 (AHT) (left) in the control simulations and (right) the anomalies (10 ka-control). Positive values indicate
 184 northward heat transport. (Middle row) Meridional mass streamfunction (MSF). Red indicates a clockwise
 185 circulation anomaly; black contours show control values. (Bottom row) Total gross moist stability (GMS)
 186 (left) in the control simulations and (right) the anomalies.

200 sponds directly to the TOA energy balance [Held and Hou, 1980], while in the winter hemi-
 201 sphere it is restricted by extratropical eddies and nonlinear momentum fluxes [Walker and Schnei-
 202 der, 2006; Merlis *et al.*, 2013a]. The Hadley circulation is to first order tied to the SST pat-
 203 tern, and is therefore strongly constrained with a fixed SST field [Singh *et al.*, 2017]. In the

204 slab ocean experiment, colder SST anomalies in the NH tropics slow the Hadley circulation.
 205 By contrast, in the fixed SSTs experiment, the NH Hadley cell in JJA does not change appreciably,
 206 though it manages to achieve a similar AHT (Fig. 4). Given that the Hadley circulation maintains its strength in the fixed SSTs experiment, the zonal mean precipitation changes
 207 very little.
 208

209 **3.2.3 Total Gross Moist Stability**

210 The total GMS is the efficiency of the export of energy by the total circulation, including the mean meridional circulation, stationary eddies, and transient eddies [*Peters et al.*, 2008].
 211 In the 10 ka simulations the total GMS increases in the NH tropics with either ocean configuration (Fig. 4). In the slab ocean case, this more than compensates for the weakened overturning strength, thus generating southward energy flux anomalies. In the fixed SSTs case, the
 212 increase in total GMS is more modest, but is large enough to balance the energy perturbation, since the Hadley circulation is unresponsive to the forcing absent SST gradient anomalies.
 213
 214
 215
 216

217 The total GMS increase is reflected in elevated equivalent potential temperature aloft, which is likely linked to changes over land in the Northern tropics, including widespread warming and increased tropospheric relative humidity (not shown). This demonstrates that even with
 218 modest surface MSE fluctuations over ocean, the zonal mean energetic stratification of the atmosphere can dominate the zonal mean climate response to forcing.
 219
 220
 221

222 This response contradicts the simplistic picture in which tropical total GMS is set by the surface meridional MSE gradient, which is constrained by the minimal (or nonexistent) SST
 223 response in the simulations. This understanding is based on two assumptions of tropical climate: that moist convection homogenizes MSE in the ascending branch of the Hadley cell, and
 224 that there is a weak temperature gradient aloft which sets the MSE in the upper Hadley cell branch to that of the ascending region [*Held*, 2001]. In this framework, the total GMS is set
 225 by the surface meridional MSE contrast across the latitudinal extent of the Hadley cell, and would not be expected to change significantly in a climate with fixed SSTs.
 226
 227
 228
 229

230 **3.3 Annual Mean Climate Response**

231 The annual mean Hadley circulation anomaly in the slab ocean experiment qualitatively resembles the JJA response, with reduced ascent north of the equator (anomaly with maximum
 232 magnitude of $20 - 25 \times 10^9 \text{ kg s}^{-1}$ or up to 40% of the climatological circulation strength;
 233

not shown). Since the branch of the cross-equatorial Hadley cell in the summer hemisphere is most responsive to radiative changes, the annual mean circulation change depends on the superposition of these solstitial changes throughout the year [Merlis *et al.*, 2013a,b]. In the 10 ka simulations, the seasonal cycle strengthens in the NH and weakens in the SH compared to the present. Therefore, the summer ascending branch changes more in JJA than DJF, and the annual mean anomaly resembles the JJA anomaly. In the slab ocean experiment only, the zonal mean cooling and drying in the northern tropics and warming and moistening in the southern tropics are also evident in the annual mean climate response, consistent with Clement *et al.* [2004]. There is not a clear annual mean ITCZ shift in the fixed SSTs experiment, which suggests that the annual mean ITCZ shift due to 10 ka orbital forcing is caused by a rectification of seasonally varying rainfall changes associated with Hadley cell dynamics, for which anomalous SST gradients are crucial.

4 Discussion

This study highlights that zonally symmetric orbital forcing can engender highly zonally asymmetric hydrological and thermal responses in the tropics. Regional differences in the temperature, MSE, and ω perturbations give rise to differing precipitation responses over the Sahel and the adjacent North Atlantic ITCZ. In both prescribed SST and slab ocean experiments, moistening over Africa in JJA is accompanied by a counterintuitive zonal mean energetic and precipitation response. The JJA zonal-mean climate is dominated by the reduced precipitation over the Northern tropical ocean.

The phasing of the Hadley cell regime and the insolation forcing determines where the circulation will be most sensitive to local energetic anomalies. Our experiments support that when SSTs are fixed, the circulation strength is constrained and the total GMS adjusts to achieve the cross-equatorial energy flux. When SSTs in a 50-meter slab ocean interact with the forcing, they are anomalously cool in the NH tropics in JJA, and result in a weaker Hadley circulation. The lag response of SSTs to insolation forcing amplifies both the regional and zonal mean JJA precipitation responses.

The results shown here are consistent with a reduced July, August, September mean Hadley cell mass flux in the Merlis *et al.* [2013a] aquaplanet experiment with 10 ka precession. It is interesting that the zonal mean circulation changes on an aquaplanet of 5-meter depth are consistent with those in our study, which includes a substantially deeper mixed layer, full con-

265 tinent geometry, and a more comprehensive representation of atmospheric physics. The re-
266 duced mass flux in the *Merlis et al.* [2013a,c] aquaplanet experiment was accompanied by an
267 increase in NH tropical precipitation, which is not the case in our simulations. In the 5-meter
268 aquaplanet experiment, the surface heat capacity is small enough that the surface temperature
269 changes are seasonally in phase with the insolation changes, driving increased surface specific
270 humidity that leads to enhanced precipitation in the NH tropical summer, despite a weaken-
271 ing of the Hadley circulation. The influence of the slab ocean depth on the SST field and the
272 associated precipitation response warrants further study. Also in contrast to our study, in sim-
273 ulations with a zonally-symmetric subtropical continent, the summer Hadley cell mass flux in-
274 creased and the ITCZ moved northward [*Merlis et al.*, 2013b,c].

275 The simple predictive model for the annual mean tropical precipitation response to or-
276 bital forcing proposed by *Bischoff, Schneider, and Meckler* [2017] does not capture the zonal
277 mean response to 10 ka orbital forcing reported here. That model predicts a strengthening of
278 NH tropical precipitation, dominated by enhanced precipitation in NH summer. The assump-
279 tion that the ITCZ position is proportional to the cross equatorial atmospheric energy flux re-
280 lies on a modest response of the total GMS, and does not account for the influence of zonal
281 inhomogeneity.

282 *Liu et al.* [2017] assessed twelve coupled model simulations with mid-Holocene orbital
283 parameters, and found that three models displayed southward ITCZ shifts, consistent with their
284 ECHAM4.6 slab ocean simulation and the results reported here. They posited that this was
285 due to radiative feedbacks or the inadequacy of the energetic framework. Our analysis sup-
286 ports the latter, in that anomalous energy transports are not, as commonly assumed, generated
287 purely through changes in overturning strength and associated ITCZ shifts.

288 It is difficult to validate any simulated zonal mean precipitation response to orbital forc-
289 ing based on available paleoclimate proxy records, due to ambiguity in whether these prox-
290 ies are tracking seasonal or annual trends, combined with the scarcity of data over the ocean
291 [*Tigheelaar and Timmermann*, 2016]. Our results show that rainfall over the Sahel is not an
292 extension of the ITCZ, so one cannot simply deduce the zonal mean climate change from lo-
293 cal proxies [*Roberts et al.*, 2017].

294 In summary, an energetics-based analysis elucidates the regional and zonal mean trop-
295 ical precipitation responses to Holocene orbital forcing. Enhanced vertical export of MSE via
296 deepening ascent intensifies rainfall over the Sahel and North Africa with 10 ka orbital param-

297 eters, even without SST changes. A southward (minimal) JJA ITCZ shift in the slab ocean (fixed
 298 SSTs) experiment is accompanied by an increase in the total GMS, and in the slab ocean ex-
 299 periment by a weakening of the Hadley circulation in the hemisphere with a brighter summer.
 300 The mechanisms we describe may provide a window into the varying hydrological responses
 301 of coupled models to Holocene orbital forcing.

302 **Acknowledgments**

303 J.E.S. was partly supported by the NOAA Ernest F. Hollings Scholarship Program. S.A.H. is
 304 supported by an NSF AGS Postdoctoral Research Fellowship, NSF Award #1624740.

305 **References**

- 306 Back, L., and C. Bretherton (2006), Geographic variability in the export of moist static
 307 energy and vertical motion profiles in the tropical Pacific, *Geophysical Research Letters*,
 308 *33*(17), doi:10.1029/2006GL026672.
- 309 Berg, A., B. Lintner, K. Findell, S. Seneviratne, and B. van den Hurk et al. (2015), In-
 310 terannual coupling between summertime surface temperature and precipitation over
 311 land: Processes and implications for climate change, *Journal of Climate*, *28*, 1308–1328,
 312 doi:10.1175/JCLI-D-14-00324.1.
- 313 Bischoff, T., T. Schneider, and A. N. Meckler (2017), A conceptual model for the
 314 response of tropical rainfall to orbital variations, *Journal of Climate*, (2017), doi:
 315 10.1175/JCLI-D-16-0691.1.
- 316 Clement, A. C., A. Hall, and A. Broccoli (2004), The importance of precessional signals
 317 in the tropical climate, *Climate Dynamics*, *22*(4), 327–341, doi:10.1007/s00382-003-
 318 0375-8.
- 319 deMenocal, P. (2015), Paleoclimate: End of the African Humid Period, *Nature Geoscience*,
 320 *8*, 86–87, doi:10.1038/ngeo2355.
- 321 DeMenocal, P., and J. Tierney (2012), Green Sahara: African humid periods paced by
 322 earth's orbital changes, *Nature Education Knowledge*, *3*(10), 12.
- 323 Donohoe, A., D. M. Frierson, and D. S. Battisti (2014), The effect of ocean mixed layer
 324 depth on climate in slab ocean aquaplanet experiments, *Climate Dynamics*, *43*(3-4),
 325 1041–1055, doi:10.1007/s00382-013-1843-4.
- 326 Emanuel, K. A. (1995), On thermally direct circulations in moist atmospheres,
 327 *Journal of the Atmospheric Sciences*, *52*(9), 1529–1534, doi:10.1175/1520-

- 328 0469(1995)052;1529:OTDCIM;2.0.CO;2.
- 329 GFDL Global Atmospheric Model Development Team (2004), The new GFDL global
 330 atmosphere and land model AM2LM2: Evaluation with prescribed SST simulations,
 331 *Journal of Climate*, 17(24), 4641–4673, doi:10.1175/JCLI-3223.1.
- 332 Held, I. (2001), The partitioning of the poleward energy transport between the tropi-
 333 cal ocean and atmosphere, *Journal of the Atmospheric Sciences*, 58, 943–948, doi:
 334 10.1175/1520-0469(2001)058;0943:TPOTPE;2.0.CO;2.
- 335 Held, I. M., and A. Y. Hou (1980), Nonlinear axially symmetric circulations in a nearly
 336 inviscid atmosphere, *Journal of the Atmospheric Sciences*, 37(3), 515–533, doi:
 337 10.1175/1520-0469(1980)037;0515:NASCIA;2.0.CO;2.
- 338 Hill, S., Y. Ming, and I. Held (2015), Mechanisms of forced tropical meridional energy
 339 flux change, *Journal of Climate*, 28, 1725–1742, doi:10.1175/JCLI-D-14-00165.1.
- 340 Hill, S. A., Y. Ming, I. M. Held, and M. Zhao (2017), A moist static energy budget–based
 341 analysis of the Sahel rainfall response to uniform oceanic warming, *Journal of Climate*,
 342 30(15), 5637–5660, doi:10.1175/JCLI-D-16-0785.1.
- 343 Hurley, J., and W. Boos (2013), Interannual variability of monsoon precipitation and lo-
 344 cal subcloud equivalent potential temperature, *Journal of Climate*, 26(23), 9507–9527,
 345 doi:10.1175/JCLI-D-12-00229.1.
- 346 Joussame, S., K. Taylor, P. Braconnot, J. Mitchell, J. Kutzbach, S. Harrison, I. Prentice,
 347 A. Broccoli, A. Abe-Ouchi, P. Bartlein, C. Bonfils, B. D'Onofrio, J. Guiot, K. Herterich,
 348 C. Hewitt, D. Jolly, J. Kim, A. Kislov, A. Kitoh, M. Loutre, V. Masson, B. McAvaney,
 349 N. McFarlane, N. de Noblet, W. Peltier, J. Peterschmitt, D. Pollard, D. Rind, J. Royer,
 350 M. Schlesinger, J. Syktus, S. Thompson, P. Valdes, G. Vettoretti, R. Webb, and U. Wy-
 351 putta (1999), Monsoon changes for 6000 years ago: Results of 18 simulations from
 352 the Paleoclimate Modeling Intercomparison Project (PMIP), *Geophys. Res. Letters*, 26,
 353 859–862, doi:10.1029/1999GL900126.
- 354 Kang, S., D. Frierson, and I. Held (2009), The tropical response to extratropical ther-
 355 mal forcing in an idealized GCM: The importance of radiative feedbacks and con-
 356 vective parameterization, *Journal of the Atmospheric Sciences*, 66, 2812–2827, doi:
 357 10.1175/2009JAS2924.1.
- 358 Liu, X., D. S. Battisti, and A. Donohoe (2017), Tropical precipitation and cross-equatorial
 359 ocean heat transport during the mid-Holocene, *Journal of Climate*, 30(10), 3529–3547,
 360 doi:10.1175/JCLI-D-16-0502.1.

- 361 Luan, Y., P. Braconnot, Y. Yu, W. Zheng, and O. Marti (2012), Early and mid-Holocene
362 climate in the tropical Pacific: Seasonal cycle and interannual variability induced by
363 insolation changes, *Climate of the Past*, pp. 1093–1108, doi:10.5194/cp-8-1093-2012.
- 364 Merlis, T., T. Schneider, S. Bordoni, and I. Eisenman (2013a), Hadley circulation response
365 to orbital precession. Part I: Aquaplanets, *J. Climate*, 26, 740–753, doi:10.1175/JCLI-D-
366 11-00716.1.
- 367 Merlis, T., T. Schneider, S. Bordoni, and I. Eisenman (2013b), Hadley circulation response
368 to orbital precession. Part II: Subtropical continent, *Journal of Climate*, 26, 754–771,
369 doi:10.1175/JCLI-D-12-00149.1.
- 370 Merlis, T., T. Schneider, S. Bordoni, and I. Eisenman (2013c), The tropical precipitation
371 response to orbital precession, *Journal of Climate*, 26, 2010–2021, doi:10.1175/JCLI-D-
372 12-00186.1.
- 373 Neelin, D., and I. Held (1987), Modeling tropical convergence based on the
374 moist static energy budget, *Mon. Wea. Rev.*, 115, 3–12, doi:10.1175/1520-
375 0493(1987)115;0003:MTCBOT;2.0.CO;2.
- 376 Patricola, and Cook (2007), Dynamics of the West African monsoon under mid-Holocene
377 precessional forcing: Regional climate model simulations, *Journal of Climate*, 20, 694–
378 716, doi:10.1175/JCLI4013.1.
- 379 Peters, M., Z. Kuang, and C. Walker (2008), Analysis of atmospheric energy transport in
380 ERA-40 and implications for simple models of the mean tropical circulation, *Journal of*
381 *Climate*, 21, doi:10.1175/2008JCLI2073.1.
- 382 Prive, and Plumb (2007), Monsoon dynamics with interactive forcing. Part I: Axisymmet-
383 ric studies, *Journal of the Atmospheric Sciences*, 64, doi:10.1175/JAS3916.1.
- 384 Reynolds, R. W., N. A. Rayner, T. M. Smith, D. C. Stokes, and W. Wang (2002), An
385 improved in situ and satellite SST analysis for climate, *Journal of Climate*, 15(13),
386 1609–1625, doi:10.1175/1520-0442(2002)015;1609:AIISAS;2.0.CO;2.
- 387 Roberts, W. H. G., P. J. Valdes, and J. S. Singarayer (2017), Can energy fluxes be used to
388 interpret glacial/interglacial precipitation changes in the tropics?, *Geophysical Research*
389 *Letters*, 44(12), 6373–6382, doi:10.1002/2017GL073103, 2017GL073103.
- 390 Schneider, T., T. Bischoff, and G. Huag (2014), Migrations and dynamics of the intertropical
391 convergence zone, *Nature Review*, 513, 45–53, doi:10.1038/nature13636.
- 392 Singh, M. S., Z. Kuang, and Y. Tian (2017), Eddy influences on the strength of the hadley
393 circulation: Dynamic and thermodynamic perspectives, *Journal of the Atmospheric*

394 *Sciences*, 74(2), 467–486, doi:10.1175/JAS-D-16-0238.1.

395 Tierney, J., S. Lewis, B. Cook, A. LeGrande, and G. Schmidt (2011), Model, proxy and
396 isotopic perspectives on the east african humid period, *Earth and Planetary Science*
397 *Letters*, 307, 103–112, doi:10.1016/j.epsl.2011.04.038.

398 Tierney, J., F. Pausata, and P. deMenocal (2017), Rainfall regimes of the green sahara,
399 *Science Advances*, 3(1), doi:10.1126/sciadv.1601503.

400 Tigchelaar, M., and A. Timmermann (2016), Mechanisms rectifying the annual mean re-
401 sponse of tropical atlantic rainfall to precessional forcing, *Climate Dynamics*, 47(1-2),
402 271–293, doi:=10.1007/s00382-015-2835-3.

403 Walker, C. C., and T. Schneider (2006), Eddy influences on hadley circulations: Simula-
404 tions with an idealized gcm, *Journal of the Atmospheric Sciences*, 63(12), 3333–3350,
405 doi:= 10.1175/JAS3821.1.